The Performance of Two Symbol Timing Recovery Algorithms for PSK Demodulators

William G. Cowley, *Member, IEEE*, and Lesley P. Sabel, *Member, IEEE*

***Abstract*— A statistical analysis of a decision-directed symbol timing algorithm for phase shift keyed modems is presented. The timing detector uses only one sample per symbol period and is suitable for high speed modems which employ discrete-time synchronization methods. Expressions for the timing detector's mean value and variance, as a function of timing offset, are derived and compared to simulation results. The analysis includes the effects of decision errors which occur at low signal-to-noise ratios and eventually limit the useful operating range of the decision-directed methods. A modification is described so that the need for prior phase recovery is avoided. These algorithms are compared to a popular two-sample-per-symbol nondecision-directed timing detector. A method of examining the relative performance of the various algorithms is presented and results are given for a range of signal-to-noise ratios and channel bandwidths.**

I. Introduction

A VARIETY of techniques are suitable for symbol timing recovery in phase shift keyed modems which operate on continuous signals (e.g., [5], [8], [2]). In the case of high-speed modems, (tens of megasymbols per second) it is likely that receive filtering will be implemented using analog filters and that the received signal will be digitized after filtering. In this paper two symbol timing algorithms which operate on the resulting samples are considered.

Fig. 1 shows a model of the system under consideration. Double lines indicate complex-valued quantities. The task of estimating the carrier phase ϕ at the receiver is not considered in this paper. Inphase and quadrature samples after receive filtering are available for the symbol timing detector. The same model applies when a numerically controlled oscillator (NCO) is used in place of a VCO. The symbol timing loops can therefore be "all digital" (e.g., [1]), or can use a hybrid approach where the time offset is derived via discrete-time processing and the sampling instant adjustment is implemented with analog circuitry (e.g., [10]).

We will examine the statistical properties of two symbol timing algorithms that are suitable for continuous PSK modems with the structure outlined above. The first algorithm considered is a one-sample-per-symbol decision-directed algorithm [2] which will be called the DD-1 algorithm. It may be written as

$$z_n = \mathrm{Re}\{x_n \hat{a}_{n-1}^* - x_{n-1}\hat{a}_n^*\} \tag{1}$$

where x_n is the nth symbol sample, and a_n is the nth transmitted symbol, with asterisk indicating complex conjugate and hat indicating that the receiver has to estimate the value of a_n (hence, the "decision directed" nature of the algorithm). Normally, the estimate of a_n is made by choosing the symbol closest to the current x_n. This approach allows a very efficient implementation.

A baseband derivation of DD-1 is given in [2] for PAM signals. However the DD-1 algorithm is suitable for any PSK signal set. The derivation in [1] follows from an approximation to the maximum likelihood estimate of the timing offset, τ, at the receiver. The decision-directed approach is attractive due to the single symbol-centered sample, particularly for high-speed applications, but decision-directed algorithms have a reputation for failing at low signal-to-noise ratios. We address this in Section II, by investigating the performance of this algorithm by analysis and simulation, taking the effect of decision errors into account.

The algorithm described above is compared to a popular nondecision-directed timing function [3] which uses two samples per symbol. This algorithm will be called NDD-2. It may be written

$$u_n = x_{n-1/2}^i(x_n^i - x_{n-1}^i) + x_{n-1/2}^q(x_n^q - x_{n-1}^q) \tag{2}$$

where the superscript indicates the inphase or quadrature component of the symbol sample, and the subscript $n-1/2$ indicates the samples lying midway between the symbol-centered samples of the $(n-1)$th and nth symbols. The model in Fig. 1 is still valid for this algorithm except that two $(T/2)$ delay elements would be used after the sampler. In Section III some new results are derived for NDD-2 and comparisons are made with DD-1.

Given an overall (real-valued) impulse response

$$g(t) = h(t) * h(-t) \tag{3}$$

the complex-valued sample of the nth symbol after receive filtering can be expressed, assuming no phase offset (i.e., $\hat{\phi} = \phi$ in Fig. 1), as

$$x_n = y_n(\boldsymbol{a}, \tau) + \nu_n \tag{4}$$

where

$$y_n(\boldsymbol{a}, \tau) = \sum_{i=-\infty}^{\infty} a_i g_{n-i}(\tau) \tag{5}$$

Paper approved by U. Mengali, the Editor for Synchronization Systems and Techniques of the IEEE Communications Society. Manuscript received November 12, 1990; revised November 25, 1991, and August 3, 1992.

W. G. Cowley is with the Signal Processing Research Institute, University of South Australia, The Levels, Pooraka, SA 5095, Australia.

L. P. Sabel is with the Australian Space Centre for Space Signal Processing, The Levels, Pooraka, SA 5095, Australia.

IEEE Log Number 9401054.

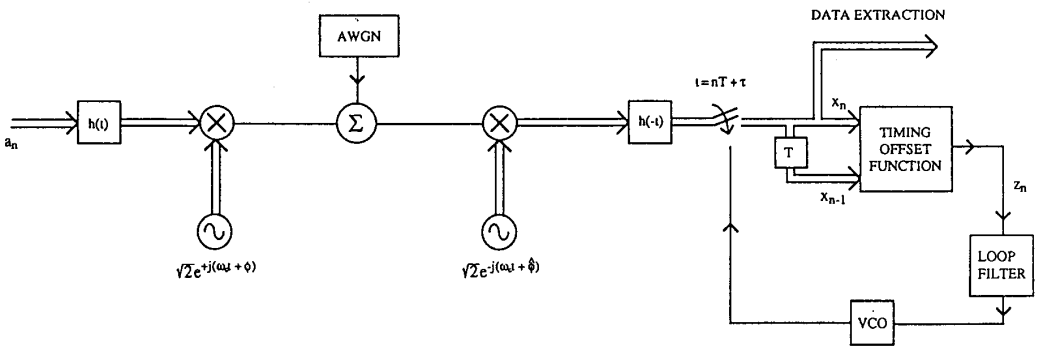

Fig. 1. Model of modem symbol timing for the decision directed algorithm.

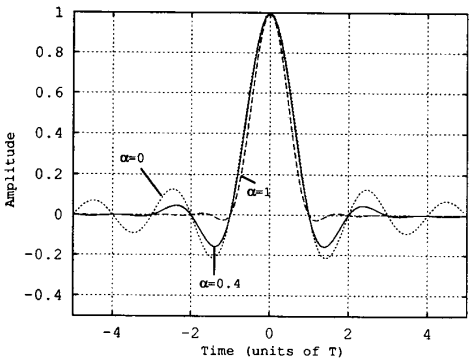

Fig. 2. Raised cosine filter impulse response $g(t)$.

with $g_{n-i}(\tau)$ denoting $g((n-i)T+\tau)$ and the noise term $\nu_n = \nu(nT+\tau)$ which is zero-mean complex-valued low-pass noise.

We assume use of the raised cosine impulse response, for which

$$g(t) = \frac{\sin(\pi t/T)\cos(\alpha\pi t/T)}{\pi t/T\,(1-(2\alpha t/T)^2)} \tag{6}$$

where α is the roll-off parameter. In the following analysis we have used the approximation that $g(t)$ can be truncated and so only a finite number of symbols will contribute to y_n. For example, from the plot of $g(t)$ in Fig. 2 it can be seen that when $|t|$ is greater than three symbol periods the value of $g(t)$ is close to zero if α is greater than about 0.4. We will denote the symbols in the vicinity of a_n by

$$\boldsymbol{a} = (a_{n-m}, a_{n-m+1}, \cdots a_{n+m}). \tag{7}$$

In some demodulators it may be desirable to make the symbol timing independent of carrier phase recovery. The NDD-2 algorithm has the property of being invariant to phase offsets but the DD-1 algorithm does not. The performance of a modified version of the decision-directed algorithm, called DD-1M, which can be used without prior carrier phase recovery, is addressed in Section IV. Section V extends some results to MPSK, particularly $M = 4$, modulation.

Finally, some brief comments are required on how the performance of timing detectors effects the overall operation of the demodulator. The simplest method of estimating timing jitter assumes that the loop is locked, and that the mean value of the timing detector (often called it's S curve) is a linear function of the sampling offset τ, with constant variance. If the timing jitter is small enough, so that uniform sampling can be assumed, the z-transform method can then be used to calculate the sampling clock variance (as in [4] or [7]). The results of the following sections describe the performance of timing detectors in terms of S curve shape and slope at the origin, and the correlation properties of the detector output. This allows timing algorithms to be compared against each other for given loop bandwidths and signal-to-noise ratios.

II. Performance of the Decision-Directed Timing Algorithm for BPSK

For comparison with later results, first consider the case of no errors in estimating $\hat{a}_n$. In this situation it is easy to determine the mean value of the DD-1 timing estimator. At this stage we are assuming BPSK, with $a_n = \pm 1$. Using (1) and (4) and replacing $\hat{a}_n^*$ by a_n,

$$\begin{aligned} E\{z_n(\tau)\} &= E\{\mathrm{Re}\{x_n a_{n-1}\}\} - E\{\mathrm{Re}\{x_{n-1}a_n\}\} \\ &= E\left\{a_{n-1}\left(\sum_i a_i g_{n-i}(\tau) + \nu_n\right)\right\} \\ &\quad - E\left\{a_n\left(\sum_i a_i g_{n-i-1}(\tau) + \nu_{n-1}\right)\right\}. \end{aligned} \tag{8}$$

Assuming that the transmitted symbols are independent the result simplifies to

$$E\{z_n(\tau)\} = g_1(\tau) - g_{-1}(\tau). \tag{9}$$

In a similar fashion an expression for the variance of z_n may be readily derived if it is assumed that no errors are made in symbol decisions. Since the a_n are real-valued, the Re operator can be dropped from the following, provided the real part of ν_n is used.

$$\begin{aligned} \mathrm{var}(z_n(\tau)) &= E\{z_n^2\} - (E\{z_n\})^2 \qquad (10) \\ &= E\{(x_n a_{n-1} - x_{n-1}a_n)^2\} \\ &\quad - (g_1(\tau) - g_{-1}(\tau))^2 \\ &= 2E\{x_n^2\} - 2E\{x_n x_{n-1} a_n a_{n-1}\} \\ &\quad - (g_1(\tau) - g_{-1}(\tau))^2. \qquad (11) \end{aligned}$$

The first term in (11) is

$$2\sum_k g_k^2(\tau) + 2\sigma^2$$

where σ^2 is the variance of real component of ν_n. The second term is

$$\begin{aligned} &-2E\left\{\left(\sum_i a_i g_{n-i}(\tau) + \nu_n\right)\right. \\ &\quad\left.\cdot\left(\sum_j a_j g_{n-1-j}(\tau) + \nu_{n-1}\right) a_n a_{n-1}\right\} \\ &= -2\sum_i\sum_j E\{a_i a_j a_n a_{n-1}\} g_{n-i}(\tau) g_{n-1-j}(\tau). \end{aligned}$$

The only nonzero terms here are when $i = n$ and $j = n-1$, and when $i = n-1$ and $j = n$, giving $-2g^2(\tau) - 2g_1(\tau)g_{-1}(\tau)$. Collecting terms, (11) simplifies to give

$$\text{var}\,(z_n(\tau)) = 2\sigma^2 + g_1^2(\tau) + g_{-1}^2(\tau) + 2\sum_{\substack{k\neq \\ -1,0,1}} g_k^2(\tau). \quad (12)$$

The first term is due to the thermal noise and the remaining terms are the "self-noise" components of the detector output. It is clear that, for Nyquist channel responses, the self-noise tends towards zero when the loop is locked.

We now consider the problem of decision errors. In reality, the $\hat{a}_n$ may not be equal to a_n due to the combined effects of noise, and ISI caused by timing offset. This is particularly true at low signal to noise ratios. We will assume that $\hat{a}_n$ is chosen simply by selecting the symbol closest to x_n. This scheme is easy to implement with a look-up table (LUT) approach (e.g., [1], [10]).

Taking the effect of decision errors into account, and assuming that the channel impulse response extends over $2m+1$ symbol periods, it is shown in Appendix A that for BPSK the mean value of the DD-1 timing detector is

$$\begin{aligned} s_D(\tau) &= E\{z_n(\tau)\} \\ &= E_{\boldsymbol{a}}\left\{\text{erf}\left(\frac{y_n(\boldsymbol{a})}{\sqrt{2}\sigma}\right)(y_{n+1}(\boldsymbol{a}) - y_{n-1}(\boldsymbol{a}))\right\} \quad (13) \end{aligned}$$

where

$$\text{erf}\,(x) = \frac{2}{\sqrt{\pi}}\int_0^x e^{-w^2}\,dw \quad (14)$$

and σ^2 is again the variance of the real component of the noise samples. (Note that erf (x) has a number of possible definitions; the erf used above is an odd function which allows some useful simplifications later on.) The notation $E_{\boldsymbol{a}}$ indicates that the expectation is only with respect to the transmitted symbols. It can easily be shown that this result is consistent with the no-decision-errors case given by (9).

Equation (13) is the S curve for the DD-1 timing detector. It has been evaluated using (A14) for the case of $\alpha = 0.4$ with $m = 3$. (Obviously a larger value of m would be required if α was smaller.) Fig. 3 shows the results as a function of σ. The curves have been labeled with the equivalent E_b/N_0 (energy per bit over single-sided noise spectral density). The relation between E_b/N_0 and σ is, (e.g., [5])

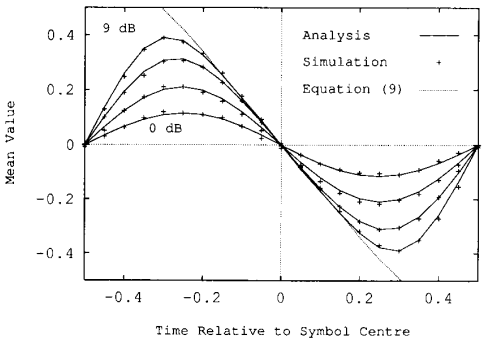

Fig. 3. DD-1 algorithm's mean value as a function of timing offset for BPSK with $E_b/N_0 = 0, 3, 6, 9$ dB, $\alpha = 0.4$.

$$E_b/N_0 = \frac{|a|^2 g^2(0)}{2\sigma^2 n_b} \quad (15)$$

where $|a|$ is the symbol magnitude (which is one in this case), $g(0) = 1$ from (6), and n_b is the number of bits per symbol. Fig. 3 shows a comparison between simulation results for the DD-1 timing detector, the theoretical values with decision errors and noise given by (13) and the ideal (no noise) values given by (9). Clearly the result given by (13) accurately models the timing detector's mean value derived from simulations. Most of the simulations referred to in this paper were carried out with the "SAT" software package [6]. Comparing the 9 dB case of (13) with the ideal case shows that decision errors only start to affect the S curve when the timing offset is greater than about $\pm 0.2\ T$.

The variance of the DD-1 timing detector with decision errors taken into account is analysed in Appendix B. The first term in (10) is shown to be

$$\begin{aligned} E\{z_n^2(\tau)\} = E_{\boldsymbol{a}}\Bigg\{ & 2y_n^2(\boldsymbol{a}) - 2\Bigg[y_n(\boldsymbol{a})y_{n-1}(\boldsymbol{a}) \\ & \cdot \text{erf}\left(\frac{y_n(\boldsymbol{a})}{\sqrt{2}\sigma}\right)\text{erf}\left(\frac{y_{n-1}(\boldsymbol{a})}{\sqrt{2}\sigma}\right) \\ & + \frac{2\sigma}{\sqrt{2\pi}}\text{erf}\left(\frac{y_n(\boldsymbol{a})}{\sqrt{2}\sigma}\right) y_n(\boldsymbol{a})(e_{n-1}(\boldsymbol{a}) + e_{n+1}(\boldsymbol{a})) \\ & + \frac{2\sigma^2}{\pi} e_n(\boldsymbol{a}) e_{n-1}(\boldsymbol{a})\Bigg]\Bigg\} + 2\sigma^2 \quad (16) \end{aligned}$$

where $e_n(\boldsymbol{a}) = e^{-y_n^2(\boldsymbol{a})/2\sigma^2}$.

Fig. 4 shows good agreement between simulations of DD-1 variance and (10), by evaluation of (13) and (16). A curve for no decision errors, corresponding to (12), has been plotted for the 9 dB case.

So far the timing detector has been considered without regard to how much correlation exists between adjacent outputs. Since the timing loop bandwidth is often a very small fraction of the symbol rate, only the lowest frequency components of the timing detector output contribute to the timing jitter. It is common to take the power spectral density (PSD) of the timing detector outputs at 0 Hz for calculations of the timing

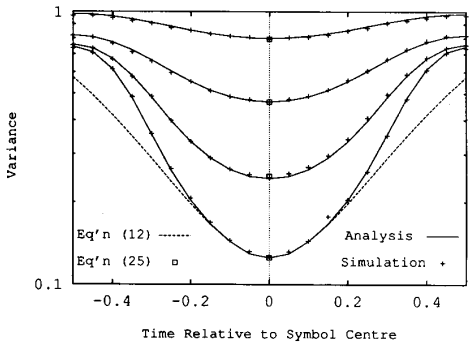

Fig. 4. DD-1 algorithm's variance as a function of timing offset for BPSK with $E_b/N_0 = 0, 3, 6, 9$ dB, $\alpha = 0.4$.

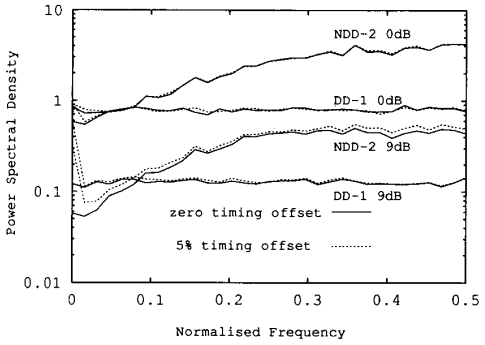

Fig. 5. Comparison of the DD-1 and NDD-2 algorithms' power spectral density at 0 and 5% timing offset as a function of frequency with $E_b/N_0 = 0$ and 9 dB, $\alpha = 0.4$.

jitter (e.g., [7]). For this reason we will analyze the correlation between timing detector outputs so that the detector's spectral density at dc can be used as a performance metric.

Let d_n be the random component of the DD-1 output for the nth symbol, i.e.,

$$d_n = z_n - E\{z_n\}. \tag{17}$$

The autocorrelation function $R_{dd}(m) = E\{d_n d_{n-m}\}$ is easy to obtain if decision errors are neglected. Neglecting terms containing $g(rT)$ where $|r| \geq 3$, gives

$$E\{d_n d_{n-1}\} = -g_1(\tau)g_{-1}(\tau) \tag{18}$$

$$E\{d_n d_{n-2}\} = -2g_2(\tau)g_{-2}(\tau). \tag{19}$$

When there are few decision errors and timing offset is close to zero, the autocorrelation function will be small for nonzero lags. For lower signal-to-noise ratios the self-noise contributions will be small compared to the thermal noise term. The d_n are therefore expected to be substantially uncorrelated when the timing loop is locked.

The power spectral density of DD-1 noise terms is given by the discrete-time Fourier transform [11]

$$S_D(\theta) = \sum_{k=-\infty}^{\infty} R_{dd}(k)e^{-j\theta k} \tag{20}$$

where θ is the normalized frequency in radians per second $2\pi f/f_s$. Using the approximation that $R_{dd}(k) = 0$ for $k \neq 0$, means that $S_D(\theta)$ will be constant and equal to $R_{dd}(0)$ (or $\text{var}(z_n)$).

Fig. 5 shows plots of the power spectrums obtained by simulations of the DD-1 and NDD-2 timing detectors at E_b/N_0 values of 0 and 9 dB, each for timing offsets of 0 and 5% of T. In all cases the decision-directed algorithm has a flat spectrum whose amplitude agrees with the levels expected from Fig. 4. This indicates that the assumptions made above concerning $R_{dd}(m)$ are reasonable. In Fig. 5 the plots were made by averaging spectral estimates of the timing detector outputs, z_n (or u_n) using 128 point periodograms [11]. When the timing offset is 5% an impulse can be seen in the measured spectrum at dc, due to the mean value of the timing detector.

In later figures the spectral density of the timing detector at dc normalized by the square of the slope of the S curve at $\tau = 0$ (i.e., $S(0)/\dot{s}^2(0)$ which we will denote $\tilde{S}(0)$), has been plotted. The normalization is required since the final sampling instant variance will be proportional to this quantity, provided that the loop bandwidth is small and constant [7]. (The normalization gives the spectral density for an equivalent timing detector whose slope is unity.) This should be a "worst case" normalization in that it assumes the loop bandwidth is fixed. In practice the loop bandwidth is proportional to the S curve slope and so would be reduced at low-signal levels. This would need to be considered in the overall system design.

Before leaving this section we will consider some simplifications in the analysis which can be made in the region of $\tau = 0$. This is obviously the location of most interest when symbol timing is "in lock." The numerical evaluation of (13) and (16) is tedious and can be bypassed when only the slope and variance of the S curve at $\tau = 0$ are needed.

Dealing first with the slope of the DD-1 detector's S curve at the origin, from (13)

$$\begin{aligned}\frac{d}{d\tau}E\{z_n(\tau)\} = E_{\boldsymbol{a}}\Bigg\{&\text{erf}\left(\frac{y_n(\boldsymbol{a},\tau)}{\sqrt{2\sigma}}\right)\\ &\cdot\sum_i a_i(\dot{g}_{n+1-i}(\tau) - \dot{g}_{n-1-i}(\tau))\Bigg\}\\ &+ E_{\boldsymbol{a}}\Bigg\{\frac{d}{d\tau}\text{erf}\left(\frac{y_n(\boldsymbol{a},\tau)}{\sqrt{2\sigma}}\right)(y_{n+1}(\boldsymbol{a},\tau)\\ &- y_{n-1}(\boldsymbol{a},\tau))\Bigg\}\end{aligned} \tag{21}$$

where $\dot{g}_k(\tau) = \frac{d}{d\tau}g(kT + \tau)$.

When $\tau = 0$, the first term in (21) becomes

$$E_{\boldsymbol{a}}\left\{\text{erf}\left(\frac{a_n}{\sqrt{2\sigma}}\right)a_n(\dot{g}_1(0) - \dot{g}_{-1}(0))\right\}$$

since the expected value of all terms with $i \neq n$ is zero. As erf( ) is an odd function, and $a_n = \pm 1$, the first term therefore simplifies to

$$\text{erf}\left(\frac{1}{\sqrt{2\sigma}}\right)(g_1(0) - \dot{g}_{-1}(0)).$$

For the second term in (21), it can be readily shown that

$$\frac{d}{d\tau}\operatorname{erf}\left(\frac{y_n(\boldsymbol{a},\tau)}{\sqrt{2}\sigma}\right)=\frac{2}{\sqrt{\pi}}e^{-y_n^2(\boldsymbol{a},\tau)/2\sigma^2}\cdot\frac{1}{\sqrt{2}\sigma}\sum_i a_i\dot{g}_{n-i}(\tau). \quad (22)$$

When $\tau = 0$, the expected value of the second part of (21) becomes

$$\frac{\sqrt{2}}{\sqrt{\pi}}\frac{1}{\sigma}e^{-1/2\sigma^2}E_{\boldsymbol{a}}\left\{\sum_i a_i\dot{g}_{n-i}(0)(a_{n+1}-a_{n-1})\right\}.$$

Collecting terms, the final result is

$$\dot{s}_D(0)=\frac{d}{d\tau}E\{z_n(\tau)\}|_{\tau=0}=\left(\operatorname{erf}\left(\frac{1}{\sqrt{2}\sigma}\right)-\frac{\sqrt{2}e^{-1/2\sigma^2}}{\sqrt{\pi}\sigma}\right)\cdot(\dot{g}_1(0)-\dot{g}_{-1}(0)). \quad (23)$$

Comparing this to the derivative of (9), the right-hand term represents the slope of the DD-1 detector S curve at the origin when no decision errors are present, and the first term indicates the relative reduction in slope due to decision errors.

The variance at the origin can be determined easily from (16). Since $E\{z_n(0)\} = 0$, and $y_n(\boldsymbol{a}, 0) = a_n$, we have

$$\operatorname{var}(z_n(0))=E_{\boldsymbol{a}}\left\{2-2\left[a_na_{n-1}\operatorname{erf}(a_n/\sqrt{2}\sigma)\cdot\operatorname{erf}(a_{n-1}/\sqrt{2}\sigma)+2\frac{\sqrt{2}\sigma}{\sqrt{\pi}}\operatorname{erf}(a_n/\sqrt{2}\sigma)a_ne^{-1/2\sigma^2}+\frac{2\sigma^2}{\pi}e^{-1/\sigma^2}\right]\right\}+2\sigma^2 \quad (24)$$

which simplifies to

$$S_D(0)=\operatorname{var}(z_n(0))=2(1-q^2)-4\frac{\sqrt{2}}{\sqrt{\pi}}\sigma qe^{-1/2\sigma^2}-\frac{4\sigma^2}{\pi}e^{-1/\sigma^2}+2\sigma^2 \quad (25)$$

where $q = \operatorname{erf}(1/\sqrt{2}\sigma)$.

Equations (23) and (25) may be easily evaluated and checked against the previous results at $\tau = 0$. We have done this for (25) at four signal-to-noise ratios and shown the results on Fig. 4 as square symbols. Evaluation of (23) gives good agreement with the slopes in Fig. 3.

III. Analysis and Comparison of the Nondecision-Directed Algorithm for BPSK

We now compare the DD-1 results with the nondecision-directed timing detector NDD-2, defined in (2). When used with BPSK with prior carrier phase recovery, only the I channel components would be used in order to reduce detector variance. Apart from the sampling rate being double that of DD-1, if the NDD-2 algorithm is precomputed via a LUT approach, three samples are required which makes the implementation slightly more difficult.

The S curve of NDD-2 for BPSK can readily be derived, using (2) and (5),

$$s_N(\tau)=E\{u_n(\tau)\}=\sum_m g_{m-1/2}(\tau)(g_m(\tau)-g_{m-1}(\tau)) \quad (26)$$

and also

$$\dot{s}_N(0)=2\dot{g}_{-1/2}+\sum_m g_{m-1/2}(\dot{g}_m-\dot{g}_{m-1}) \quad (27)$$

where $g_m = g_m(0) = g(mT)$. It can be seen that the S curve depends only on the channel impulse response and (unlike DD-1) is not affected by the signal-to-noise ratio. (A detailed derivation of the S curve in the frequency domain [3] gives insight into the effect of different channel bandwidths.)

When the variance of NDD-2 is examined via simulation, plots similar in shape to those of Fig. 4 are obtained showing the typical self noise plus thermal noise contributions. In order to compare the two detectors on the basis of normalised spectral density at dc, the correlation properties of NDD-2 must be examined. In this case adjacent samples of the timing detector are significantly correlated and consequently its spectral density is not flat.

To follow the same approach as before, let c_n represent the random component of the nth NDD-2 output, i.e.,

$$c_n = u_n - E\{u_n\}. \quad (28)$$

The correlation analysis for NDD-2 appears to be difficult in the general case. However, when the timing offset is zero, results for $E\{c_nc_{n-m}\}$ may be derived which illustrate the correlation and power spectrum of the detector. We have simulated the effect of small timing offsets on the NDD-2 spectrum and found little difference between $\tau = 0$ and 5% of T (see Fig. 5). Appendix C contains an outline of the analysis of NDD-2's correlation properties when $\tau = 0$. As we are most interested in the detector's noise spectrum at dc, let

$$S_N(0)=\sum_k R_{cc}(k)$$

and from the results in (C10), (C11), and (C12), using the approximation that $R_{cc}(m)$ will remain the same when $\tau \cong 0$, gives

$$S_N(0)\cong 2(\sigma^2+\sigma^4)\left(1-\sum_{m=1}^{\infty}(g_{m-1/2}-g_{m+1/2})^2\right). \quad (29)$$

This result is surprisingly simple considering the correlation analysis for NDD-2. Although the $R_{cc}(m)$ are nonzero, even for the no-noise case, all the noise independent terms cancel out when the autocorrelations are summed to form $S_{cc}(0)$, i.e., there is no self-noise at $f = 0$. The σ^4 term is due to noise times noise terms and so represents the squaring loss associated with the nondecision-directed scheme. The term in large brackets depends on the roll-off factor and evaluates to 0.3802 when $\alpha = 0.4$.

It is important to describe how these timing functions are affected by different channel bandwidths. The results given in Figs. 3, 4, and 5 assume an α of 0.4 which was chosen due to its widespread use. However, the timing detectors are

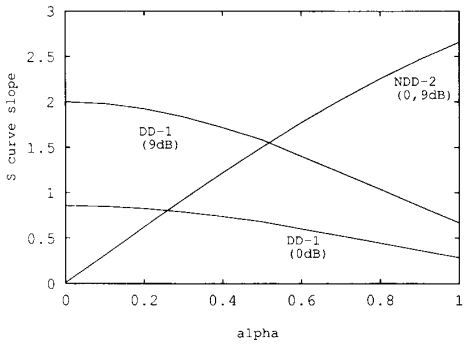

Fig. 6. Comparison of the DD-1 and NDD-2 algorithms' S curve slope as a function of α for BPSK at $E_b/N_0 = 0$ and 9 dB.

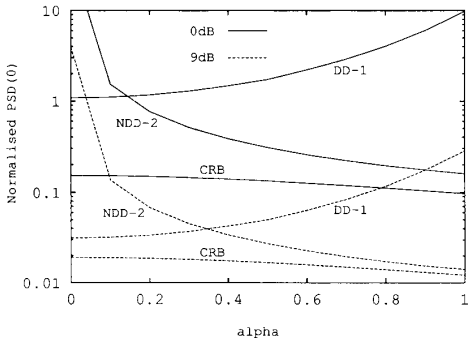

Fig. 7. Comparison of the DD-1 and NDD-2 algorithms' normalized power spectral density at dc and the Cramer–Rao bound as a function of α for BPSK at $E_b/N_0 = 0$ and 9 dB.

quite sensitive to the roll-off factor and behave differently as it varies. As pointed out in [3] the NDD-2 algorithm operates better as α increases. The timing detector slope and normalized PSD at dc for zero timing offset have been plotted for the DD-1 and NDD-2 detectors in Figs. 6 and 7 as a function of α. These figures assume BPSK with no phase offset, a normalized symbol rate ($T = 1$) and fixed $E_b/N_0 s$ of 0 and 9 dB, respectively. The DD-1 results are via evaluation of (23) and (25) while the NDD-2 results are from (27) and (29). We have checked these predictions with simulations at $\alpha = 0.1$, 0.4, and 0.8 and found good agreement.

We have also plotted a lower bound on the figures which represents the Cramer–Rao Bound on variance of timing estimates [7], [12] for independent known symbols at the receiver. As the number of symbols becomes large, the variance per symbol is

$$\sigma^2_{\mathrm{CRB}} = \left(\frac{2}{N_0} a_n^2 \int_{-\infty}^{\infty} (2\pi f)^2 |H(f)|^2 \, df\right)^{-1}. \quad (30)$$

The integral term depends on the shape of the channel impulse response and may be shown to be equal to $-\ddot{g}(0)$. The bound is only mildly affected by the roll-off factor, as seen from the figures.

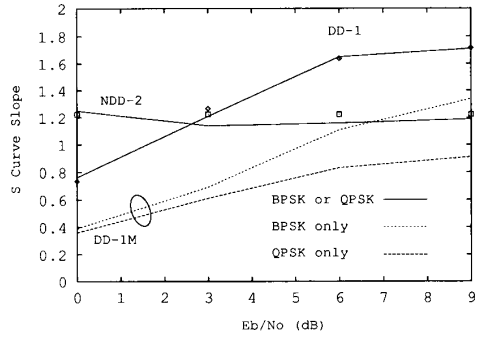

Fig. 8. Comparison of the magnitude of the DD-1 and NDD-2 algorithms' S curve slope with no phase offset and the DD-1M algorithm with $f_o = 0.0011$ cycles per symbol as a function of E_b/N_0 for BPSK and QPSK, $\alpha = 0.4$, $\tau = 0$.

IV. Performance of Timing Algorithms for BPSK without Prior Phase Recovery

Modems that use differentially coherent demodulation, or require independent carrier and timing synchronization, must use a timing offset detector which is insensitive to phase offsets. The NDD-2 algorithm has this desirable attribute [3], provided that both the real and imaginary components of data samples in (2) are employed.

The DD-1 timing detector will not operate usefully with an arbitrary phase offset. However the phase offset can be estimated from the two samples x_n and x_{n-1}, and the samples rotated before (1) is evaluated. In effect this is a simple form of prior phase recovery. Since only x_n and x_{n-1} are used in the estimation of phase offset, the whole sequence of phase estimation, sample rotation and timing offset estimation may be precomputed and stored in a fast LUT. Although the performance is degraded due to the high phase error variance, the approach allows phase independent, one-sample-per-T symbol timing to be implemented very easily. For example, it has been used in a flexible PSK demodulator which operates to 85 Msymbol/s [10].

We will denote the algorithm described above as DD-1M. We used a nondecision-directed phase estimator [9] for the phase estimation operation in DD-1M. Simulations shows that its S curve resembles the plots in Fig. 3 but the amplitude is reduced by about one third. DD-1M's performance, together with the other timing algorithms, is summarized in Figs. 8–10 at the end of the paper.

V. Timing Algorithm Performance for MPSK, $M > 2$

In this section we will extend the previous results, where possible, to higher order PSK signal sets. This includes expressions for the mean and variance of the DD-1 timing detector in a number of cases, and comparison of DD-1, DD-1M, and NDD-2 results by simulation.

First consider DD-1 with no phase offset or decision errors in symbol estimates, and MPSK modulation where $M > 2$. The nth transmit symbol can be represented as

$$a_n = e^{j2\pi L_n/M} \quad \text{with } L_n \in \{0, 1, \cdots, M-1\}. \quad (31)$$

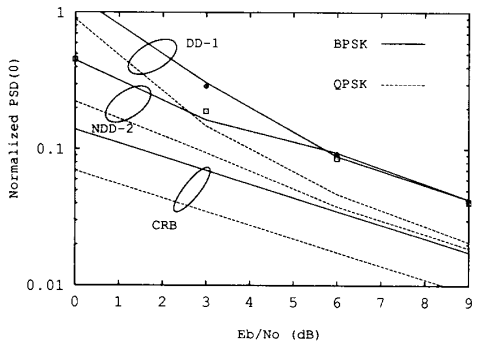

Fig. 9. Comparison of the algorithms' normalized PSD(0) and the CRB as a function of E_b/N_0 for BPSK and QPSK with no phase offset, $\alpha = 0.4$.

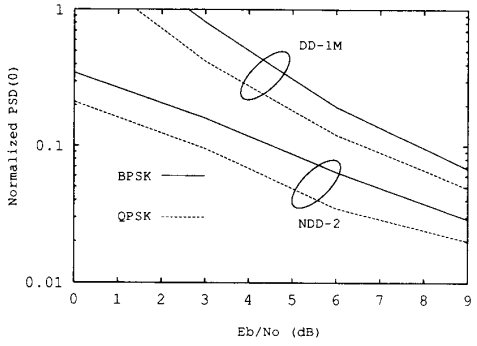

Fig. 10. Comparison of the algorithms' normalized PSD(0) as a function of E_b/N_0 for BPSK and QPSK, $\alpha = 0.4$, $f_o = 0.0011$ cycles per symbol.

Replacing a_{n-1} and a_n in (8) by a^*_{n-1} and a^*_n, and since, for example,

$$E\{\mathrm{Re}\{a^*_{n-1}a_i\}\} = 1 \quad \text{if } i = n-1$$
$$= 0 \quad \text{otherwise,}$$

after simplification, the same S curve expression is obtained, i.e., (9).

Under similar assumptions an expression for the variance of z_n may be derived. This time, using $\mathrm{Re}\{c\} = (c + c^*)/2$, we can write

$$E\{z_n^2\} = E\{1/4(x_n a^*_{n-1} + x^*_n a_{n-1} - x_{n-1}a^*_n - x^*_{n-1}a_n)^2\}. \quad (32)$$

The expression may be expanded in a similar fashion to Section II. The result is

$$\mathrm{var}(z_n(\tau)) = 2\sigma^2 + (g_1^2(\tau) + g_{-1}^2(\tau))/2 + \sum_{\substack{k\neq \\ -1,0,1}} g_k^2(\tau). \quad (33)$$

It can be seen that the self-noise components are half those of the BPSK case in (12). The thermal noise contributions, for fixed E_b/N_0 and constant magnitude symbols, are also smaller as the number of bits per symbol increases, as shown by (15).

We will now examine the performance of the DD-1 algorithm specifically for QPSK ($M = 4$) at low signal-to-noise ratios when there is no phase offset. Here we can take advantage of the fact that QPSK is equivalent to orthogonal BPSK signal sets. Denoting real and imaginary components of x_n by $x_n = x_n^I + jx_n^Q$, and likewise for a_n and ν_n, then (1) becomes

$$z_n = \mathrm{Re}\{(x_n^I + jx_n^Q)(a^I_{n-1} - ja^Q_{n-1}) - (x^I_{n-1} + jx^Q_{n-1})(a_n^I - ja_n^Q)\}$$
$$= (x_n^I a^I_{n-1} - x^I_{n-1}a_n^I) + (x_n^Q a^Q_{n-1} - x^Q_{n-1}a_n^Q). \quad (34)$$

Furthermore, from (5),

$$x_n^I = \sum_i a_i^I g((n-i)T + \tau) + \nu_n^I$$

and similarly for x_n^Q. The two terms in (34) are therefore independent and each is equivalent to the case considered in Section II. After taking signal and noise scaling factors into account, it is found that the S curves in the QPSK case are the same, and the variance is reduced by a factor of 2. This is in accordance with the error-free MPSK results given earlier. As expected for DD-1M, the S curve slope for QPSK is reduced compared to BPSK.

The timing detector performance is summarized (for $\alpha = 0.4$) in Figs. 8, 9, and 10. The S curve slope at $\tau = 0$, $\dot{s}(0)$, and normalized PSD at dc, $\tilde{S}(0)$, are plotted. In Fig. 10 the frequency offset was the same as that used in Section IV (0.0011 cycles per symbol period). For each figure, lines show simulation results and nearby symbols show values predicted from (23), (25), (27), and (29). Two versions of the lower bound (30) have also been plotted on Fig. 9.

VI. Conclusion

New results have been derived for the one-sample-per-symbol decision-directed timing detector, DD-1, concerning the S curve and detector variance at low signal-to-noise ratios. The performance has been compared to the two-sample-per-symbol nondecision-directed algorithm, NDD-2, which required an analysis of its correlation properties.

Results presented in figures provide some indication of how the performance of DD-1 degrades at lower signal-to-noise ratios due to decision errors. For example from Fig. 9, at $\alpha = 0.4$, the DD-1 and NDD-2 approaches could be expected to give about the same timing jitter at an E_b/N_0 of 6 dB. At 3 dB, the standard deviation of the timing jitter in the one-sample-per-T DD-1 system would be worse by approximately 25%. Without prior phase recovery, for BPSK at 6 dB the DD-1M would have approximately 75% more timing jitter than the two-sample-per-T system, for the same loop bandwidth. Finally, it should be remembered that channel bandwidth has a major effect on the relative performance of these schemes, as indicated in Figs. 6 and 7.

Appendix A
Mean Value of the DD-1 Algorithm for BPSK with No Phase Offset

We require the expected value of z_n. Since BPSK is assumed, $a_n = \pm 1$. From (1)

$$E\{z_n(\tau)\} = E\{x_n\hat{a}_{n-1}\} - E\{x_{n-1}\hat{a}_n\} \quad \text{(A1)}$$

where x and $\hat{a}$ are both functions of the transmitted symbols and the noise samples.

Assuming that x_n is a function of the limited range of symbols denoted by $\boldsymbol{a}$ in (7), as well as ν_n, the first term above is

$$E\{x_n\hat{a}_{n-1}\} = \int\int\int p_{A,N}(\boldsymbol{a}, \nu_n, \nu_{n-1})(y_n(\boldsymbol{a}) + \nu_n) \cdot \hat{a}_{n-1}\, d\nu_{n-1}\, d\nu_n\, d\boldsymbol{a} \quad \text{(A2)}$$

where $p_{A,N}(\cdot)$ is the joint probability density function of the discrete valued transmitted symbols and the continuous valued noise samples. We have simplified the notation of $y_n(\boldsymbol{a})$ from (4). All integration limits are from $-\infty$ to $+\infty$ unless otherwise shown. The integration with respect to $\boldsymbol{a}$ represents multiple integrations over each of the independent symbols that contribute to $\boldsymbol{a}$. The symbol estimate $\hat{a}_{n-1}$ is a function of y_{n-1} and ν_{n-1} according to the rule

$$\begin{aligned}\hat{a}_{n-1} &= 1 \quad \text{if } y_{n-1}(\boldsymbol{a}) + \nu_{n-1} > 0 \\ &= -1 \quad \text{otherwise.}\end{aligned} \quad \text{(A3)}$$

We can therefore split (A2) into

$$\begin{aligned}E\{x_n\hat{a}_{n-1}\} = &\int\int\int_{-y_{n-1}}^{\infty} p_{A,N}(\boldsymbol{a}, \nu_n, \nu_{n-1}) \\ &\cdot (y_n(\boldsymbol{a}) + \nu_n)\, d\nu_{n-1}\, d\nu_n\, d\boldsymbol{a} \\ &- \int\int\int_{-\infty}^{-y_{n-1}} p_{A,N}(\boldsymbol{a}, \nu_n, \nu_{n-1}) \\ &\cdot (y_n(\boldsymbol{a}) + \nu_n)\, d\nu_{n-1}\, d\nu_n\, d\boldsymbol{a}. \end{aligned} \quad \text{(A4)}$$

Now consider the form of the joint density function used above. The transmitted symbols are independent and identically distributed. The real-valued noise samples are Gaussian distributed, with variance σ^2. In addition the samples ν_n and ν_{n-1} are independent due to the symbol spaced sampling and the use of root Nyquist receive filters, see (C6). We may therefore write the joint density function as

$$p_{A,N}(\boldsymbol{a}, \nu_n, \nu_{n-1}) = p_A(\boldsymbol{a}) p_N(\nu_n) p_N(\nu_{n-1}) \quad \text{(A5)}$$

where

$$p_N(\nu_n) = (2\pi\sigma^2)^{-1/2} e^{-\nu_n^2/2\sigma^2} \quad \text{(A6)}$$

and

$$\begin{aligned}p_A(\boldsymbol{a}) = 2^{-(2m+1)} \sum_{\forall \boldsymbol{\alpha}} &\delta(\alpha_1 - a_{n-m}) \\ &\cdot \delta(\alpha_2 - a_{n-m+1}) \cdots \delta(\alpha_{2m+1} - a_{n+m})\end{aligned} \quad \text{(A7)}$$

such that $\boldsymbol{\alpha} = (\alpha_1, \alpha_2 \cdots \alpha_{2m+1})$ with $\alpha_i \in \{-1, +1\}$ for $i = 1, \cdots 2m+1$. The summation in (A7) is over all possible values of the set of transmitted symbols that are assumed to contribute to the current sample x_n, i.e., $\boldsymbol{\alpha}$ can take on 2^{2m+1} values from $(-1, -1, -1, \cdots -1)$ to $(1, 1, 1, \cdots 1)$.

Using (A5) and (A6) in the first term of (A4) and rearranging, gives

$$\begin{aligned}\int p_A(\boldsymbol{a}) \int p_N(\nu_n)(y_n(\boldsymbol{a}) + \nu_n) \\ \cdot \int_{-y_{n-1}(\boldsymbol{a})}^{\infty} (2\pi\sigma^2)^{-1/2} e^{-\nu_{n-1}^2/2\sigma^2}\, d\nu_{n-1}\, d\nu_n\, d\boldsymbol{a}.\end{aligned} \quad \text{(A8)}$$

The innermost integral, using (14), is equal to $\frac{1}{2}\left(1 + \text{erf}\left(\frac{y_{n-1}(\boldsymbol{a})}{\sqrt{2}\sigma}\right)\right)$

We can therefore write the first term of (A4) as

$$\int p_A(\boldsymbol{a}) \frac{1}{2}\left(1 + \text{erf}\left(\frac{y_{n-1}(\boldsymbol{a})}{\sqrt{2}\sigma}\right)\right) \int p_N(\nu_n)(y_n(\boldsymbol{a}) + \nu_n)\, d\nu_n\, d\boldsymbol{a}. \quad \text{(A9)}$$

It can be seen that the additive noise term ν_n in this expression will not contribute to the final result (since $E\{\nu_n\} = 0$). The integral of $p_N(\nu_n)$ from $-\infty$ to ∞ is 1, so we are left with

$$\int p_A(\boldsymbol{a}) y_n(\boldsymbol{a}) \frac{1}{2}\left(1 + \text{erf}\left(\frac{y_{n-1}(\boldsymbol{a})}{\sqrt{2}\sigma}\right)\right) d\boldsymbol{a}. \quad \text{(A10)}$$

In a similar way the second term of (A4) can be evaluated. Now the innermost integral in (A8) becomes $\frac{1}{2}\left(1 - \text{erf}\left(\frac{y_{n-1}(\boldsymbol{a})}{\sqrt{2}\sigma}\right)\right)$.

The first and second terms of (A4) can therefore be combined to give

$$\int p_A(\boldsymbol{a}) y_n(\boldsymbol{a}) \,\text{erf}\left(\frac{y_{n-1}(\boldsymbol{a})}{\sqrt{2}\sigma}\right) d\boldsymbol{a}. \quad \text{(A11)}$$

So far we have only dealt with the first term of (A1). The second term may be handled by noting that since

$$\begin{aligned}E\{x_n\hat{a}_{n-1}\} &= E\{x_{n+1}\hat{a}_n\} \\ &= \int p_A(\boldsymbol{a}) y_{n+1}(\boldsymbol{a}) \,\text{erf}\left(\frac{y_n(\boldsymbol{a})}{\sqrt{2}\sigma}\right) d\boldsymbol{a}\end{aligned} \quad \text{(A12)}$$

so from symmetry

$$E\{x_{n-1}\hat{a}_n\} = \int p_A(\boldsymbol{a}) y_{n-1}(\boldsymbol{a}) \,\text{erf}\left(\frac{y_n(\boldsymbol{a})}{\sqrt{2}\sigma}\right) d\boldsymbol{a}$$

hence, overall

$$E\{z_n(\tau)\} = E_{\boldsymbol{a}}\left\{\text{erf}\left(\frac{y_n(\boldsymbol{a})}{\sqrt{2}\sigma}\right)(y_{n+1}(\boldsymbol{a}) - y_{n-1}(\boldsymbol{a}))\right\}. \quad \text{(A13)}$$

The expectation in (A13) is only with respect to transmitted symbols. It may be evaluated for different values of τ by choosing an appropriate value of m to limit the number of symbols in $\boldsymbol{a}$ and using (A7) and the property of delta functions to give

$$\begin{aligned}E\{z_n(\tau)\} = 2^{-(2m+1))} \sum_{\forall \boldsymbol{\alpha}} \\ \cdot \text{erf}\left(\frac{y_n(\boldsymbol{\alpha})}{\sqrt{2}\sigma}\right)(y_{n+1}(\boldsymbol{\alpha}) - y_{n-1}(\boldsymbol{\alpha}))\end{aligned} \quad \text{(A14)}$$

where $\boldsymbol{\alpha}$ takes on all of the 2^{2m+1} possible values.

Appendix B
Variance of the DD-1 Algorithm for BPSK with no Phase Offset

In order to determine the variance of the DD-1 algorithm the expectation $E\{z_n^2(\tau)\}$ must be determined. The variance is

$$\text{var}\,(z_n(\tau)) = E\{z_n^2(\tau)\} - (E\{z_n(\tau)\})^2 \quad \text{(B1)}$$

where $E\{z_n(\tau)\}$ has been determined in Appendix A.

From (1) and (4)

$$E\{z_n^2(\tau)\} = E\{x_n^2\} - 2E\{x_n x_{n-1}\hat{a}_n\hat{a}_{n-1}\} + E\{x_{n-1}^2\} \tag{B2}$$

$$E\{x_n^2\} = E\{y_n^2(\boldsymbol{a})\} + 2E\{y_n\}E\{\nu_n\} + E\{\nu_n^2\} \tag{B3}$$

$$= E\{y_n^2(\boldsymbol{a})\} + \sigma^2 \tag{B4}$$

as y_n and ν_n are independent, and as ν_i has zero mean and σ^2 variance. In addition

$$E\{x_n^2\} = E\{x_{n-1}^2\}. \tag{B5}$$

Now $E\{x_n x_{n-1}\hat{a}_n\hat{a}_{n-1}\}$ is a function of y_n, y_{n-1}, ν_n, and ν_{n-1}. As $\hat{a}_n\hat{a}_{n-1}$ can take on values 1 and -1, the expectation can be separated into 2 parts:

$$\hat{a}_n\hat{a}_{n-1} = 1 \quad \text{called region 1 defined as}$$

$$(\hat{a}_n = 1 \quad \text{and} \quad \hat{a}_{n-1} = 1) \quad \text{or} \quad (\hat{a}_n = -1 \quad \text{and} \quad \hat{a}_{n-1} = -1)$$

which may be written as

$$(y_n(\boldsymbol{a}) + \nu_n > 0 \quad \text{and} \quad y_{n-1}(\boldsymbol{a}) + \nu_{n-1} > 0) \quad \text{region 1a} \tag{B6}$$

or

$$(y_n(\boldsymbol{a}) + \nu_n < 0 \quad \text{and} \quad y_{n-1}(\boldsymbol{a}) + \nu_{n-1} < 0) \quad \text{region 1b} \tag{B7}$$

and

$$\hat{a}_n\hat{a}_{n-1} = -1 \quad \text{called region 2 defined as}$$

$$(\hat{a}_n = 1 \quad \text{and} \quad \hat{a}_{n-1} = -1) \quad \text{or} \quad (\hat{a}_n = -1 \quad \text{and} \quad \hat{a}_{n-1} = 1)$$

which may be likewise be written

$$(y_n(\boldsymbol{a}) + \nu_n > 0 \quad \text{and} \quad y_{n-1}(\boldsymbol{a}) + \nu_{n-1} < 0) \quad \text{region 2a} \tag{B8}$$

or

$$(y_n(\boldsymbol{a}) + \nu_n < 0 \quad \text{and} \quad y_{n-1}(\boldsymbol{a}) + \nu_{n-1} > 0) \quad \text{region 2b.} \tag{B9}$$

So $E\{x_n x_{n-1}\hat{a}_n\hat{a}_{n-1}\}$ becomes $E\{x_n x_{n-1}\}$ evaluated over region 1 minus $E\{x_n x_{n-1}\}$ on region 2.

Evaluating $E\{x_n x_{n-1}\}$ on region 1a, and using the same notation as (A2),

$$E\{x_n x_{n-1}\}|_{1a} = \int\int_{-y_n}^{\infty}\int_{-y_{n-1}}^{\infty} p_{A,N}(\boldsymbol{a}, \nu_n, \nu_{n-1})(y_n(\boldsymbol{a}) + \nu_n) \cdot (y_{n-1}(\boldsymbol{a}) + \nu_{n-1})\, d\nu_{n-1}\, d\nu_n\, d\boldsymbol{a}. \tag{B10}$$

Similarly

$$E\{x_n x_{n-1}\}|_{1b} = \int\int_{-\infty}^{-y_n}\int_{-\infty}^{-y_{n-1}} p_{A,N}(\boldsymbol{a}, \nu_n, \nu_{n-1})(y_n(\boldsymbol{a}) + \nu_n) \cdot (y_{n-1}(\boldsymbol{a}) + \nu_{n-1})\, d\nu_{n-1}\, d\nu_n\, d\boldsymbol{a}. \tag{B11}$$

The evaluation for region 2 takes a similar form. Expanding (B10) first,

$$E\{x_n x_{n-1}\}|_{1a} = \int\int_{-y_n}^{\infty}\int_{-y_{n-1}}^{\infty} p_A(\boldsymbol{a})p_N(\nu_n)p_N(\nu_{n-1}) \cdot (y_n(\boldsymbol{a})y_{n-1}(\boldsymbol{a}) + y_n(\boldsymbol{a})\nu_{n-1} + y_{n-1}(\boldsymbol{a})\nu_n + \nu_n\nu_{n-1})\, d\nu_{n-1}\, d\nu_n\, d\boldsymbol{a} \tag{B12}$$

and using the same assumptions as in part A, this becomes

$$\begin{aligned}
&\int p_A(\boldsymbol{a})y_n(\boldsymbol{a})y_{n-1}(\boldsymbol{a})\int_{-y_n(\boldsymbol{a})}^{\infty}(2\pi\sigma^2)^{-1/2}e^{-\nu_n^2/2\sigma^2} \\
&\quad\cdot\int_{-y_{n-1}(\boldsymbol{a})}^{\infty}(2\pi\sigma^2)^{-1/2}e^{-\nu_{n-1}^2/2\sigma^2}\, d\nu_{n-1}\, d\nu_n\, d\boldsymbol{a} \\
&\quad+\int p_A(\boldsymbol{a})y_n(\boldsymbol{a})\int_{-y_n(\boldsymbol{a})}^{\infty}(2\pi\sigma^2)^{-1/2}e^{-\nu_n^2/2\sigma^2} \\
&\quad\cdot\int_{-y_{n-1}(\boldsymbol{a})}^{\infty}(2\pi\sigma^2)^{-1/2}e^{-\nu_{n-1}^2/2\sigma^2}\nu_{n-1}\, d\nu_{n-1}\, d\nu_n\, d\boldsymbol{a}. \\
&\quad+\int p_A(\boldsymbol{a})y_{n-1}(\boldsymbol{a})\int_{-y_n(\boldsymbol{a})}^{\infty}(2\pi\sigma^2)^{-1/2}e^{-\nu_n^2/2\sigma^2}\nu_n \\
&\quad\cdot\int_{-y_{n-1}(\boldsymbol{a})}^{\infty}(2\pi\sigma^2)^{-1/2}e^{-\nu_{n-1}^2/2\sigma^2}\, d\nu_{n-1}\, d\nu_n\, d\boldsymbol{a} \\
&\quad+\int p_A(\boldsymbol{a})\int_{-y_n(\boldsymbol{a})}^{\infty}(2\pi\sigma^2)^{-1/2}e^{-\nu_n^2/2\sigma^2}\nu_n \\
&\quad\cdot\int_{-y_{n-1}(\boldsymbol{a})}^{\infty}(2\pi\sigma^2)^{-1/2}e^{-\nu_{n-1}^2/2\sigma^2}\nu_{n-1}\, d\nu_{n-1}\, d\nu_n\, d\boldsymbol{a}.
\end{aligned} \tag{B13}$$

It may be shown that

$$\int_{-y_{n-1}}^{\infty}(2\pi\sigma^2)^{-1/2}e^{-\nu_{n-1}^2/2\sigma^2}\nu_{n-1}\, d\nu_{n-1} = \sigma(2\pi)^{-1/2}e^{-y_{n-1}^2(\boldsymbol{a})/2\sigma^2}.$$

To simplify notation let

$$e_{n-1}(\boldsymbol{a}) = e^{-y_{n-1}^2(\boldsymbol{a})/2\sigma^2}. \tag{B14}$$

Using the erf( ) result after (A8), (B13) can be written as

$$\begin{aligned}
E\{x_n x_{n-1}\}|_{1a} = \int p_A(\boldsymbol{a})\Bigg[&y_n(\boldsymbol{a})y_{n-1}(\boldsymbol{a})\frac{1}{2} \\
&\cdot\left(1+\operatorname{erf}\left(\frac{y_n(\boldsymbol{a})}{\sqrt{2}\sigma}\right)\right)\frac{1}{2}\left(1+\operatorname{erf}\left(\frac{y_{n-1}(\boldsymbol{a})}{\sqrt{2}\sigma}\right)\right) \\
&+y_n(\boldsymbol{a})\frac{1}{2}\left(1+\operatorname{erf}\left(\frac{y_n(\boldsymbol{a})}{\sqrt{2}\sigma}\right)\right)\frac{\sigma}{\sqrt{2\pi}}e_{n-1}(\boldsymbol{a}) \\
&+y_{n-1}(\boldsymbol{a})\frac{1}{2}\left(1+\operatorname{erf}\left(\frac{y_{n-1}(\boldsymbol{a})}{\sqrt{2}\sigma}\right)\right)\frac{\sigma}{\sqrt{2\pi}}e_n(\boldsymbol{a}) \\
&+\frac{\sigma^2}{2\pi}e_n(\boldsymbol{a})e_{n-1}(\boldsymbol{a})\Bigg]\, d\boldsymbol{a}.
\end{aligned} \tag{B15}$$

The other regions as defined by (B7) through (B9) are evaluated as per region 1a and when combined result in

$$E\{x_n x_{n-1}\hat{a}_n\hat{a}_{n-1}\} = \int p_A(\boldsymbol{a})\Bigg[y_n(\boldsymbol{a})y_{n-1}(\boldsymbol{a}) \cdot \operatorname{erf}\left(\frac{y_n(\boldsymbol{a})}{\sqrt{2}\sigma}\right)\operatorname{erf}\left(\frac{y_{n-1}(\boldsymbol{a})}{\sqrt{2}\sigma}\right) + \frac{2\sigma}{\sqrt{2\pi}}y_n(\boldsymbol{a})e_{n-1}(\boldsymbol{a})\operatorname{erf}\left(\frac{y_n(\boldsymbol{a})}{\sqrt{2}\sigma}\right) + \frac{2\sigma}{\sqrt{2\pi}}y_{n-1}(\boldsymbol{a})e_n(\boldsymbol{a})\operatorname{erf}\left(\frac{y_{n-1}(\boldsymbol{a})}{\sqrt{2}\sigma}\right) + \frac{4\sigma^2}{2\pi}e_n(\boldsymbol{a})e_{n-1}(\boldsymbol{a})\Bigg]\,d\boldsymbol{a}. \quad \text{(B16)}$$

When (B16) is written as an expectation and combined with (B4) and (B5) we have

$$E\{z_n^2(\tau)\} = E_{\boldsymbol{a}}\Bigg\{2y_n^2(\boldsymbol{a}) - 2\Bigg[y_n(\boldsymbol{a})y_{n-1}(\boldsymbol{a}) \cdot \operatorname{erf}\left(\frac{y_n(\boldsymbol{a})}{\sqrt{2}\sigma}\right)\operatorname{erf}\left(\frac{y_{n-1}(\boldsymbol{a})}{\sqrt{2}\sigma}\right) + \frac{2\sigma}{\sqrt{2\pi}}\operatorname{erf}\left(\frac{y_n(\boldsymbol{a})}{\sqrt{2}\sigma}\right)y_n(\boldsymbol{a})(e_{n-1}(\boldsymbol{a}) + e_{n+1}(\boldsymbol{a})) + \frac{2\sigma^2}{\pi}e_n(\boldsymbol{a})e_{n-1}(\boldsymbol{a})\Bigg]\Bigg\} + 2\sigma^2. \quad \text{(B17)}$$

This formula may be evaluated numerically for different values of τ by replacing the expectation with a summation over all possible values of $\boldsymbol{\alpha}$ containing 2^{2m+1} symbols [as for (A14)].

Appendix C
Correlation Analysis for NDD-2 for BPSK and Zero Timing Offset

An outline will be given of how an expression for the correlation between output samples of the NDD-2 timing detector can be derived for the special case when $\tau = 0$. We require $E\{c_n c_{n-m}\}$ where c_n is defined in (28).

Since BPSK with no phase offset is assumed, the quadrature component of (2) is omitted. As $\tau = 0$, $E\{u_n\} = 0$ so $c_n = u_n$, hence

$$\begin{aligned} R_{cc}(m) &= E\{u_n u_{n-m}\} \\ &= E\{x_{n-1/2}(x_n - x_{n-1})x_{n-m-1/2}(x_{n-m} - x_{n-m-1})\} \\ &= E\{x_{n-1/2}x_{n-m-1/2}(x_n x_{n-m} - x_{n-1}x_{n-m} \\ &\quad - x_n x_{n-m-1} + x_{n-1}x_{n-m-1})\}. \end{aligned} \quad \text{(C1)}$$

The four terms which contribute to this equation can be written as

$$\pm E\{x_{n-1/2}x_{n-m-1/2}x_{n-r}x_{n-m-s}\} \quad \text{(C2)}$$

where $r, s \in \{0, 1\}$ and the sign should be + if $r = s$ and − if $r \neq s$. Now consider the symbol midpoint samples in this equation, i.e., x_n, x_{n-1}, etc. As $\tau = 0$, we see from Section I of the paper that only one symbol contributes to these samples, for example $x_n = a_n + \nu_n$. The general term can therefore be written, using (5),

$$E\Bigg\{\Bigg(\underbrace{\sum_i a_i g_{n-1/2-i}}_{(s_1)} + \underbrace{\nu_{n-1/2}}_{(n_1)}\Bigg) \cdot \Bigg(\underbrace{\sum_j a_j g_{n-m-1/2-j}}_{(s_2)} + \underbrace{\nu_{n-m-1/2}}_{(n_2)}\Bigg) \cdot \underbrace{(a_{n-r}}_{(s_3)} + \underbrace{\nu_{n-r}}_{(n_3)})(\underbrace{a_{n-m-s}}_{(s_4)} - \underbrace{\nu_{n-m-s}}_{(n_4)})\Bigg\} \quad \text{(C3)}$$

where the label s_1 indicates the first signal component, n_1 is the first noise component, etc.

When (C3) is expanded, a sum of 16 product terms is produced. The all-signal product term is

$$E\{s_1 s_2 s_3 s_4\} = E\Bigg\{a_{n-r}a_{n-m-s}\sum_i a_i g_{n-1/2-i}\sum_j a_j g_{n-m-1/2-j}\Bigg\}. \quad \text{(C4)}$$

As the symbols are uncorrelated and equal to ± 1, the only contributions are shown in (C5a-c) below.

$$\text{if } r = m + s \quad \text{and} \quad i = j \quad \text{we get} \quad \sum_n g_{n-1/2}g_{n-m-1/2} \quad \text{(C5a)}$$

$$\text{if} r \neq m + s, \quad i = n - r \quad \text{and} \quad j = n - m - s \quad \text{we get} \quad g_{r-1/2}g_{s-1/2} \quad \text{(C5b)}$$

$$\text{if } r \neq m + s, \quad j = n - r \quad \text{and} \quad i = n - m - s \quad \text{we get} \quad g_{s+m-1/2}g_{r-m-1/2}. \quad \text{(C5c)}$$

Note that since (r, s) take on the 4 possible values (0, 0), (0, 1), (1, 0) and (1, 1) in each evaluation of $R_{cc}(m)$, then (C5a) will only contribute to the autocorrelation when $m = -1, 0, 1$. On the other hand, (C5b) and (C5c) must be considered in $R_{cc}(m)$ for all values of m. However, considering (C5b) when (say) $m = 2$, since $g_{-1/2} = g_{1/2}$, it can be noted that the contribution arising when $(r, s) = (0, 0)$ will be cancelled by the contribution when $(r, s) = (0, 1)$ (since the latter must be subtracted while the former is added.) Thus, (C5b) will not contribute when $|m| > 1$.

Of the signal times noise terms, all the 8 terms with one signal or one noise component must have an expected value of zero. Of the remaining 6 terms with two signal and two noise components, first it is easy to show that

$$E\{\nu(t)\nu(t + t_1)\} = \sigma^2 g(t_1) \quad \text{(C6)}$$

where $\sigma^2 = E\{\nu^2(t)\}$ as before, then

$$E\{s_3 s_4 n_1 n_2\} = \sigma^2 \quad \text{if } m = 0 \quad \text{and } r = s \quad \text{(C7a)}$$

$$E\{s_1 s_2 n_3 n_4\} = \sum_n g_{n-1/2}g_{n-m-1/2}\sigma^2 \quad \text{if } r = s + m \quad \text{(C7b)}$$

$$E\{s_1 s_4 n_2 n_3\} = E\{s_2 s_3 n_1 n_4\} = g_{s+m-1/2}g_{r-m-1/2}\sigma^2 \quad \text{(C7c)}$$

$$E\{s_1 s_3 n_2 n_4\} = E\{s_2 s_4 n_1 n_3\} = g_{r-1/2} g_{s-1/2} \sigma^2. \quad \text{(C7d)}$$

All the components represented by (C7d) will cancel out for the reasons indicated above. Similarly, (C7c) will not contribute when $m = 0$, (C7a) will only contribute when $m = 0$, etc.

Finally, the last product term from (C3) will be the all-noise term. Using the identity [13]

$$\begin{aligned} &E\{\nu_{n-1/2}\nu_{n-m-1/2}\nu_{n-r}\nu_{n-m-s}\} \\ &\quad = E\{\nu_{n-1/2}\nu_{n-m-1/2}\}E\{\nu_{n-r}\nu_{n-m-s}\} \\ &\qquad + E\{\nu_{n-1/2}\nu_{n-r}\}E\{\nu_{n-m-1/2}\nu_{n-m-s}\} \\ &\qquad + E\{\nu_{n-1/2}\nu_{n-m-s}\}E\{\nu_{n-m-1/2}\nu_{n-r}\} \quad \text{(C8)} \end{aligned}$$

the first part of this gives

$$\sigma^4 \quad \text{if } m = 0 \quad \text{and } r = s \quad \text{(C9a)}$$

while the last two components give

$$g_{r-1/2} g_{s-1/2} \sigma^4 + g_{s+m-1/2} g_{r-m-1/2} \sigma^4. \quad \text{(C9b)}$$

Expressions for the desired autocorrelations can now be written down by inspection, after considering all the terms represented by (C5), (C7) and (C9). All values of r and s must be taken into account, as indicated above, for the particular value of m being considered. For $m = 0$ the result is therefore

$$R_{cc}(0) = 2\sum_n g_{n-1/2}^2 - 4g_{1/2}^2 + 2\sigma^2\left(1 + \sum_n g_{n-1/2}^2\right) + 2\sigma^4. \quad \text{(C10)}$$

The first factor of 2 in this equation arises since $(r, s) = (0, 0)$ and $(1, 1)$ both satisfy (C5a). The next factor of -4 is caused by $(r, s) = (0, 1), (1, 0)$ satisfying both (C5b) and (C5c), and in each case $r \neq s$ so all the terms are negative. For the σ^2 terms, only (C7a) and (C7b) give a net contribution, whilst for the σ^4 terms only (C9a) appears in (C10). In a similar manner the results for other values of lag are

$$\begin{aligned} R_{cc}(1) &= 2g_{1/2}g_{3/2} + g_{1/2}^2 - g_{3/2}^2 - \sum_n g_{n-1/2}g_{n+1/2} \\ &\quad + \sigma^2\left(4g_{1/2}g_{3/2} - 2g_{1/2}^2 - 2g_{3/2}^2 \right. \\ &\quad \left. - \sum_n g_{n-1/2}g_{n+1/2}\right) \\ &\quad + \sigma^4(2g_{1/2}g_{3/2} - g_{1/2}^2 - g_{3/2}^2) \quad \text{(C11)} \end{aligned}$$

$$\begin{aligned} R_{cc}(m) &= (2g_{m-1/2}g_{m+1/2} - g_{m-1/2}^2 - g_{m+1/2}^2) \\ &\quad \cdot (1 + 2\sigma^2 + \sigma^4) \quad \text{if } |m| > 1. \quad \text{(C12)} \end{aligned}$$

REFERENCES

[1] W. G. Cowley, I. S. Morrison, and D. C. Lynes, "Digital signal processing algorithms for a phase shift keyed modem," in *Proc. ISSPA '87*, Brisbane, Aug. 1987, pp. 836–841.

[2] K. H. Mueller and M. Muller, "Timing recovery in digital synchronous data receivers," *IEEE Trans. Commun.*, vol. COM-24, pp. 516–530, May 1976.

[3] F. M. Gardner, "A BPSK/QPSK timing-error detector for sampled data receivers," *IEEE Trans. Commun.*, vol. COM-34, pp. 423–429, May, 1986.

[4] W. C. Lindsey and C. M. Chie, "A survey of digital phase-locked loops," *Proc. IEEE*, vol. 69, pp. 410–431, Apr. 1981.

[5] J. G. Proakis, *Digital Communications*. New York: McGraw-Hill, 1989, 2nd ed.

[6] R. J. Sault, A. P. Kalcina, and D. J. Skellern, "A software environment for satellite link simulations and modelling," in *Proc. Second Nat. Space Symp.*, Sydney, Australia, 1983.

[7] M. Moeneclaey, "A simple lower bound on the linearized performance of practical symbol synchronizers," *IEEE Trans. Commun.*, vol. COM-31, pp. 1029–1032, Sept. 1983.

[8] L. E. Franks, "Carrier and bit synchronization in data communications—A tutorial review," *IEEE Trans. Commun.*, vol. COM-28, pp. 1107–1120, Aug. 1980.

[9] A. J. Viterbi and A. M. Viterbi, "Nonlinear estimation of PSK-modulated carrier phase with application to burst digital transmission," *IEEE Trans. Inform. Theory*, vol. IT-29, pp. 543–551, July 1983.

[10] G. Bolding, W. G. Cowley, and I. S. Morrison, "A flexible 85 MSym/s demodulator for earth resource satellite applications," in *Proc. IREECON*, Sydney, Australia, Sept. 1991.

[11] R. A. Roberts and C. T. Mullis, *Digital Signal Processing*. Reading, PA: Addison-Wesley, 1987.

[12] R. E. Blahut, *Principles and Practice of Information Theory*. Reading, PA: Addison-Wesley, 1987.

[13] W. B. Davenport, *Probability and Random Processes*. New York: McGraw-Hill, 1970.

[14] M. Moeneclaey and T. Batselé, "Carrier independent NDA symbol synchronization for MPSK operating at only one sample per symbol," in *Proc. GLOBECOM 90*, San Diego, CA, Dec. 1990, paper 407.2.

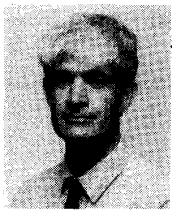

William G. Cowley (M'78) received the B.Sc., B.E., and Ph.D. degrees from the University of Adelaide in 1975, 1976, and 1985, respectively.

From 1979 to 1983 he worked on radar signal processing, at the Defence Research Centre in Salisbury, South Australia. He is currently a Senior Lecturer at the University of South Australia and a member of the Digital Communications Group. He is Deputy Director of the Australian Space Centre for Signal Processing. His interests include modem signal processing, low-rate speech coding, radar signal processing, spectral estimation techniques and real-time signal processing implementation methods.

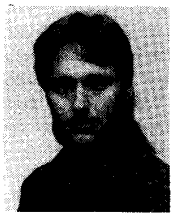

Lesley P. Sabel (M'88) was born in Salisbury, South Australia, in 1958. He received the B.Eng. degree and a Graduate Diploma in electronic systems design from the South Australian Institute of Technology in 1980 and 1985 respectively. He is currently pursuing a Ph.D. degree at the University of South Australia.

From 1980 to 1987 he worked as an electronic engineer in a number of public and private telecommunications based companies including Telecom Australia and Lane Telecommunications Consultants. Between 1987 and 1990 he was a senior engineer for Communications Division, Electronic Research Laboratories, Defence Science and Technology Organisation, South Australia where he received a scholarship to complete a Ph.D. in 1990. His current research interests include synchronisation and digital signal processing techniques for digital communications, communications theory, and spread-spectrum communication systems.